01 Apr 2002

CFD of Multiphase Flow in Packed-Bed Reactors: I. K-Fluid Modeling Issues

Y. Jiang

M. R. Khadilkar

M. (Muthanna) H. Al-Dahhan
Missouri University of Science and Technology, aldahhanm@mst.edu

M. P. Dudukovic

Recommended Citation

Y. Jiang et al., "CFD of Multiphase Flow in Packed-Bed Reactors: I. K-Fluid Modeling Issues," *AIChE Journal*, vol. 48, no. 4, pp. 701 - 715, Wiley; American Institute of Chemical Engineers (AIChE), Apr 2002.
The definitive version is available at https://doi.org/10.1002/aic.690480406

CFD of Multiphase Flow in Packed-Bed Reactors: I. *k*-Fluid Modeling Issues

Y. Jiang, M. R. Khadilkar, M. H. Al-Dahhan, and M. P. Dudukovic
Chemical Reaction Engineering Laboratory (CREL), Dept. of Chemical Engineering,
Washington University, St. Louis, MO 63130

The Eulerian k-fluid CFD model was used to simulate the macroscale multiphase flow in packed beds. The geometric complexity of the bed structure is resolved by statistically describing the porosity distribution. The complicated multiphase interactions are computed using the Ergun type of formula developed based on bench-scale hydrodynamic experiments. The work is presented in two sequential articles. Part I discusses implementation issues of the k-fluid CFD model for packed beds. The drag exchange coefficients are obtained from the model of Holub et al. for the particle-fluid interfaces X_{ks} and from the model of Attou et al. (1999) for the gas–liquid interface, X_{gl}. The effect of particle external wetting on flow distribution was incorporated into the model through the capillary pressure evaluated by either the J-function of Leverett (1941) for air–water or by the expression of Attou and Ferschneider (1999) for other fluids. In the framework of CFDLIB, the choice of the grid size and boundary conditions are discussed. An appropriate relationship between the section size and variance of the sectional porosity distribution was used for flow simulation. Part II discusses the extensive numerical results, and the CFD model is compared with experimental data in the literature.

Introduction and Background

Fluid dynamics in multiphase reactors

The performance of multiphase reactors, in principle, can be predicted by solving the conservation equations for mass, momentum, and (thermal) energy in combination with the constitutive equations for species transport, chemical reaction, and phase transition. However, because of the incomplete understanding of the physics plus the highly coupled and nonlinear nature of the equations, it is difficult to obtain the complete solution unless one has reliable physical models, advanced numerical algorithms, and sufficient computational power. Hence, in the past several decades, approaches based on residence-time distribution (RTD), together with the macromixing and micromixing models, have been the primary tool in reactor modeling used to characterize the nonideal flow pattern and mixing in reactors without solving the complete velocity field (Levenspiel, 1972). The disadvantage of such approaches is that they cannot be adopted well to serve as a diagnostic tool for operating units, which normally need to be operated under conditions not amenable to the preceding simplified analysis. To improve the capability of multiphase reactor models, one has to solve the complete multidimensional flow equations coupled with chemical species transport, reaction kinetics, and kinetics of phase change. Fortunately, computational fluid dynamics (CFD) has made great progress during the last few years, and has been applied to chemical processes (Trambouze, 1993; Kuipers and van Swaaij, 1998). In particular, one of the promising methods is the so-called full-probability density-function (PDF) model for single-phase reactive-flow systems (Fox, 1996). For most multiphase reactive-flow systems, however, the challenge still exists in both numerical technique and physical understanding of multiphase interactions. Some progress has been made for multiphase cold-flow systems and few reac-

Correspondence concerning this article should be addressed to M. P. Dudukovic.
Present addresses of: Y. Jiang, Conoco Inc., 1000 South Pine St., Ponca City, OK 74602; M. R. Khadilkar, GE Plastics, 1 Lexan Lane, Mt. Vernon, IN 47620.

tive-flow systems via CFD modeling. The features and the challenges encountered in the current CFD modeling of multiphase reactors have been reviewed by Kuipers and van Swaaij (1998), who clearly indicate that more effort is needed in applications of CFD in gas–liquid stirred tanks, gas–liquid–solid packed beds (such as trickle beds), gas–liquid–solid fluidized beds, and slurry reactors. In this study, we focus on the development of a CFD model for multiphase flow in packed-bed reactors.

Modeling approaches to multiphase flow in packed beds

Packed beds have been extensively used in petroleum, petrochemical, and biochemical applications (Duduković et al., 1999). The stationary packing in the columns can be either active catalyst for chemical-reaction systems or an adsorbent in separation columns. Depending upon the application, there are multiple configurations available for packed beds with gas and liquid flows: cocurrent downward flow (that is, trickle bed), cocurrent upward flow (that is, packed bubble column), and countercurrent flow (such as catalytic distillation column). The criteria for choosing the proper flow direction have been established, and the evaluation of the effect of flow direction on reactor performance has also been performed (Wu et al., 1996; Khadilkar et al., 1996). Since most of these models rely on assumed ideal flow patterns and are one dimensional, the accurate prediction of the multiphase flow pattern (i.e., spatial and temporal distributions) in packed beds is still an unresolved issue, which is an obstacle to advanced reactor-model development.

Multiphase flow modeling in packed beds is a challenging task because of the difficulty incorporating the complex geometry (e.g., tortuous interstices) into the flow equations, and the difficulty in accounting for the fluid–fluid (gas–liquid) interactions in the presence of complex fluid–particle (e.g., partial wetting) contacting. Moreover, until recently, the lack of noninvasive experimental techniques suitable for validating the numerical results was also a detrimental factor in numerical model development.

The earliest flow models of packed beds focused on the bed-scale flow pattern without considering the detailed heterogeneities of the bed structure. The "diffusion" model (Stanek and Szekely, 1974) and porous media model (Anderson and Sapre, 1991) are examples of such an approach. To account for the statistical nature of the bed structure, a "percolation-based" model was adopted to predict the flow pattern in packed beds (Crine et al., 1979). All of these models provided predictions of the overall quantities (usually upon tuning the model parameter) that were found comparable with the experiments; however, they could not yield much insight into the flow distribution in the beds. A discrete-cell-model (DCM) approach evolved from the assumption made by Holub (1990) that flow distribution is governed by the minimum total energy dissipation rate. In the recently updated DCM (Jiang et al., 1999), a statistical assignment of sectional porosity values and the incorporation of the interfacial tension force related to the particle external wetting and inflow distributors has been accomplished for two-phase flow in trickle beds. The quantitative predictions of the liquid upflow distribution in packed beds by the DCM approach compare well with the available experimental data and other independent numerical methods (Jiang et al., 2000). However, the numerical scheme of multivariable nonlinear minimization used in DCM often leads to low computational efficiency when dealing with a large packed bed with small cell dimensions.

Direct numerical simulation (DNS) on a single particle and single void scale requires complete characterization of the solids boundaries and voids configuration, which is difficult to obtain for a massive packed bed. Statistic description of the porosity distribution for a large-size packed bed seems appropriate for modeling of the macroscopic flow field. For example, to consider the interactions between the fluid and particles, a global flow model in packed beds, an Eulerian *k*-fluid model, resulting from the volume averaging of the continuity and momentum equations, has been developed and solved for a one-dimensional (1-D) representation of the bed at steady state, and at isothermal nonreaction conditions (Attou et al., 1999). This model provided reasonable predictions for global hydrodynamic quantities such as liquid holdup and pressure drop. A similar *k*-fluid model, based on the relative permeability concept, was used to compute the 2-D flow without considering porosity variation and without solving for the solid phase. The simulated liquid flow pattern qualitatively agreed with experimental observation (Anderson and Sapre, 1991). It seems that the Eulerian *k*-fluid model is a rational choice for flow simulation in packed beds, if good closures for fluid–fluid and fluid–particle interactions can be found and used. Moreover, the geometrical complexity of packed beds can in a certain sense be avoided in a *k*-fluid model, since there is no need to deal with the exact boundaries of the particles and since one treats the solid phase as a penetrated continuum.

A study has been made to resolve the flow field at fine scale and CFD simulations were conducted of heat transfer in a tubular fixed bed using a 3-D fine mesh within the void space (Logtenberg and Dixon, 1998). These simulations were limited to the tube with very low column-to-particle-diameter ratio ($D_r/d_p = 2 \sim 3$) and with large particle size (e.g., 5 cm). Obviously, it is impossible to adopt such an approach for a massive commercial packed bed, or even for a bench-scale trickle bed packed with small particles (such as $0.5 \sim 3$ mm). Hence, one has to discover a practical way to implement the bed structure into the flow model. It is most desirable to retain all the statistical characteristics of the void space, but without introducing the real void structure, since the exact 3-D interstitial void structure varies with repacking the bed, even with the same particles and using the same packing method, although the mean porosity and some higher moments of the voidage distribution may retain the same value.

In this work, we introduce a statistical description of the bed structure into a multiphase *k*-fluid model (that is, Eulerian–Eulerian model) framework. In order to properly consider the effect of the solid phase on gas and liquid flows, the *k*-fluid model is applied to the gas, liquid, and solid phases simultaneously, while forcing the solid to be a stationary phase, so that the initial volume fraction distribution of the solid phase is retained, and the porosity distribution of the packed bed is fixed.

The work accomplished is presented in two related articles. In this first article (Part I), various issues related to the *k*-fluid model implementation in packed beds are discussed,

and the current state of the art for closures is presented. The multiscale and statistical nature of flow is illustrated and the choice of the grid size and boundary conditions are discussed. The second article (Part II) (Jiang et al., 2002) presents selected numerical simulation results based on the model outlined in Part I, discusses the comparison of the numerical results with available experimental data, and recommends a methodology for utilizing the modeling results in packed-bed reactor analysis and design.

Spatial and Temporal Characteristics of Flow in Packed Beds

There are many structures and numerous flow parameters responsible for the flow distribution in packed beds, such as porosity distribution in the bed and the inlet flow velocity distribution (Jiang et al., 1999). For example, in a packed bed saturated with single-phase flow (such as the gas flow or liquid upflow case), the spatial variation of porosity is the essential parameter in determining the spatial distributions of fluid velocity. In a packed bed with gas and liquid two-phase flow, the additional parameters affecting the liquid distribution and phase-volume fraction variations are the state of particle external wetting, the interaction between phases, distributor design, and so on. It is believed that there exists a quantitative relation between the flow field, bed structure, and operating conditions of the system. Moreover, since the flow distribution/maldistribution can be observed at different spatial scales (Melli et al., 1990; Wang et al., 1998), it has been suggested that different scales be used to describe the various flow phenomena. This so-called multiscale nature of the flow in packed beds results from the multiscale heterogeneities of the bed structure.

In packed beds, two complementary spaces coexist: the grain space and the porous space (that is, cavity). The pore size, defined by the radius of the largest sphere, which can be placed inside that cavity, depends on particle size, shape, and packing method. For porosities of 0.36 to 0.4 obtained in cylindrical beds of monosize spheres, the pore size is in the range of $0.38R$ to $0.44R$ (R: radius of the particle). As reported in several studies on packed beds, the mean porosity is reproducible for a given packing method with a standard deviation of only 0.0016 (Cumberland and Crawford, 1987). The longitudinally averaged radial porosity profile follows a certain oscillatory pattern due to the confines of the walls, which can be predicted in terms of particle size, shape, and column-to-particle-diameter ratio (Benenati and Brosilow, 1962; Mueller, 1991; Bey and Eigenberger, 1997). Although typical bed structural information such as that just given is available, this is not sufficient to predict the complete spatial distribution of flow in packed beds. Additional information on porosity distribution in 3-D or at least 2-D, information on wall effects, entrance, and exit effects are needed before going on to flow simulation.

For both steady state and dynamic-flow simulation in packed beds, the temporal behavior of the flow has to be considered. In a two-phase flow trickle bed, in which gas is the continuous phase, whereas liquid is trickling down through the packing (that is, trickle bed) at low superficial velocity, the so-called "trickle-flow regime" in the literature, the bed-scale liquid flow pattern is rather stable, whereas the local scale interstitial flow within the void space still fluctuates in a chaotic manner. Once the gas and liquid superficial velocities increase to a certain level, and the flow reaches the so-called "high interaction pulsing regime," even the macroscale liquid pattern becomes unstable: the liquid-rich zone and gas-rich zone move alternately through the bed with a certain frequency. Such a macroscale flow fluctuation pattern also can be generated through the periodic input of the flows, which has been shown to enhance the reactor performance (Khadilkar et al., 1999).

The experimental exploration of these spatial and temporal flow variations in packed beds is definitely important, but it is difficult for a single technique to capture both the spatial and temporal behavior of flow simultaneously with high temporal and spatial resolutions (Reinecke et al., 1998). For example, magnetic resonance imaging (MRI) can provide a good spatial resolution of 0.02–0.3 mm, but it is not suitable to measure dynamics of the flow such as these encountered in the pulsing flow regime due to the temporal resolution problem. The electric capacitance tomography (ECT) gives a temporal resolution of a millisecond, but with relatively poor spatial resolution at this stage (Reinecke et al., 1998). On the numerical flow modeling side, a similar trend exists. We do not expect to use a single model to obtain flow information on a variety of spatial and temporal scales, but we should be able to obtain one level of flow information through one particular model. In these two articles, we focus on the macroscale flow pattern at steady-state operating conditions. We also explore the dynamic flow behavior of macroscale structures under periodic operating condition by including flow modulation to examine the possible improvement of the liquid distribution, but we do not model the flow dynamics in the natural pulsing flow regime, which involves complex flow dynamic mechanisms (Tsochatzidis and Karabelas, 1998).

Structure Implementation

The implementation of the porosity distribution in flow simulation increases the level of difficulty in packed beds as compared to other multiphase reactors. So far, this issue has been tackled in a deterministic and simplified manner to a large extent. For example, either uniform porosity or the radial porosity variation is considered in the model of the bed (Bey and Eigenberger, 1997; Yin et al., 2000). In some cases, a multizone porosity assignment was used (Stanek, 1994). Since the 3-D interstitial void space varies with repacking the bed, the porosity distribution possesses a statistical nature (Wijngaarden and Westerterp, 1992), and the use of statistical description of the porosity structure in the flow model has considerable potential for success (Crine et al., 1992). In this section we discuss how to partition the 3-D packed bed into sections and what will be the type of the sectional porosity distribution, since in the flow simulation of a volume-averaged k-fluid model, one needs to assign the initial solid-phase volume fraction to each section. Depending on the section size chosen for the partition, the sectional porosity values follow a certain probability density function (p.d.f). That means that the p.d.f. is section-size dependent. For example, the measured section porosity data from a cylindrical column packed with 3-mm monosize spheres exhibit a Gaussian distribution at a section-size of 3 mm (Chen et al., 2001). How-

ever, a nearly binomial distribution of sectional porosity distribution is found by MRI measurement at a section size of 180 μm (Sederman, 2000).

In principle, a quantitative relationship of the section size and the standard deviation of section porosity distribution, σ_B, can be developed through extensive MRI measurements of packed beds. Obviously, this relationship can vary with particle shape and packing method. Thus, for a certain section size, a set of pseudo random section porosities can be generated based on the following constraints:

- Mean porosity (measurable)
- Longitudinally averaged radial porosity profile (correlation available)
- Probability density function of the sectional porosity distribution for a given section size (obtainable by MRI, Sederman, 2000).

Figure 1a shows a sample contour plot of 2-D sectional porosity distribution in *r-z* coordinates, which was generated under three constraints: (1) a mean porosity of 0.36 for the whole set of sectional porosity values; (2) a longitudinally averaged radial porosity profile $[\bar{\epsilon}(r) = (1/H)\int_o^H \epsilon(r,z)\ dz]$ based on the data given by Stephenson and Stewart (1986) (see blank circles in Figure 1b); (3) Gaussian p.d.f. for each column of sectional porosity values with a mean, $\mu(r)\,[=\bar{\epsilon}(r)]$ and a standard deviation, $\sigma(r)\,[=0.12\,\mu(r)]$ (see Figure 1c). The tail shown at the high porosity range in Figure 1c indicates the effect of walls on porosity.

Constraint (3) is definitely needed because it allows us to use the statistical information (that is, probability density function) on sectional porosity distribution in describing the structure of the bed. The relationship between the statistical parameters [e.g., $\mu(r)$ and $\sigma(r)$] and the section size has also been accounted for. Although the example used provided an illustration for a 2-D case, the approach is applicable for the 3-D porosity distribution case.

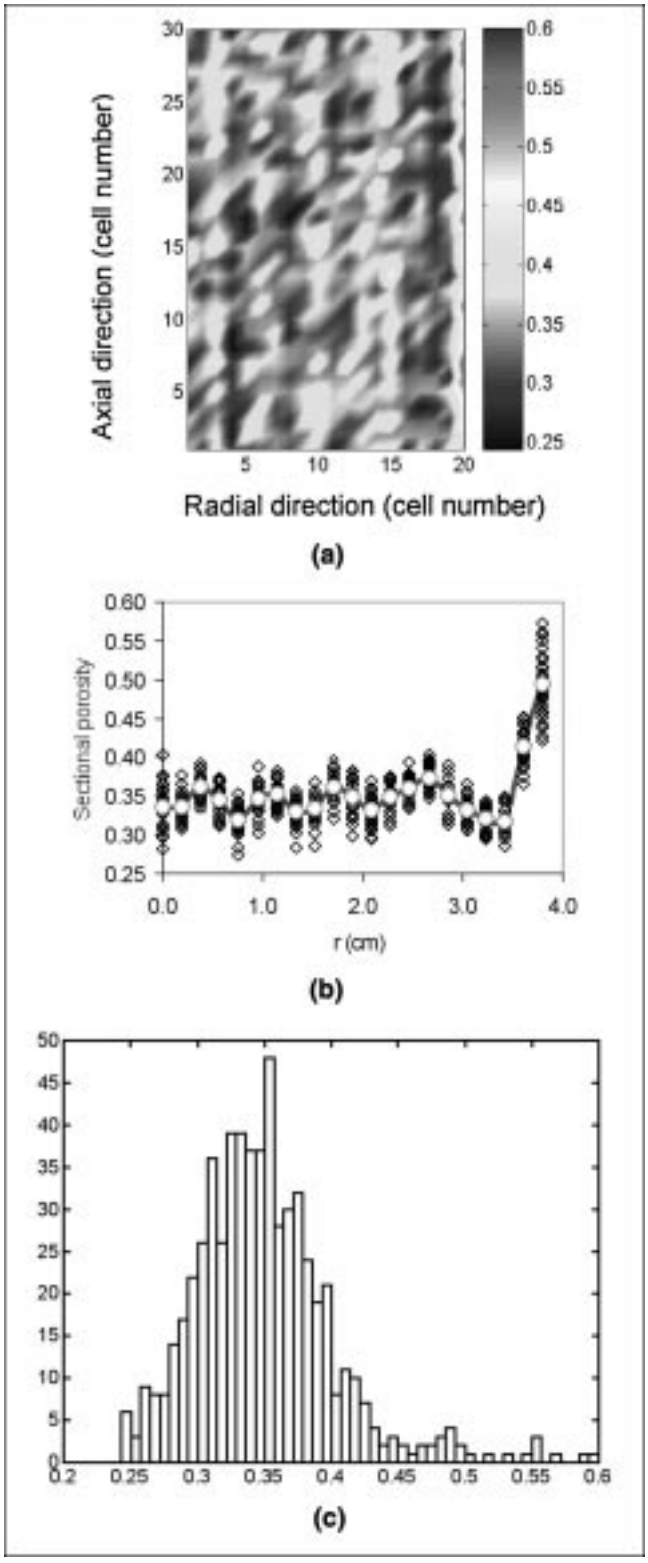

Figure 1. Generated pseudo-Gaussian distribution of porosity under three constraints.

$D_r = 7.6$ cm, $d_p = 0.703$ cm, section size $= 0.05R = 0.19$ cm. (a) Contour plot of all generated sectional porosity values; (b) radial profiles of the generated sectional porosity and longitudinally averaged radial porosity profile (blank circles) reported by Stephen and Stewart (1986); (c) histogram plot of all generated sectional porosity values.

k-Fluid Model Implementation in CFDLIB

Eulerian k-fluid model

In the Eulerian *k*-fluid approach, the different phases or materials are treated mathematically as interpenetrating continua (Ishii, 1975, Drew, 1983). The derivation of the conservation equations for mass, momentum, and enthalpy is performed by using either the volume-averaging or ensemble-averaging technique to describe the time-dependent motion of fluids and track the volume fraction distribution of each phase. In the ensemble-averaging technique, the probability of occurrence of any one phase in multiple realizations of the flow is given by the instantaneous volume fraction of that phase at that point. The sum total of all volume fractions at a point is identically unity (Anderson and Jackson, 1967).

Due to the averaging of the flow variables over a certain volume, we expect to obtain only a large-scale (averaging volume) flow structure using a *k*-fluid volume-averaged model. The microscopic flow structure below this scale, such as a detailed local flow structure, is only achievable by direct numerical simulation (DNS), which is limited to relatively low Reynolds and Schmidt numbers (Kuipers and van Swaaij, 1998). Since DNS is not possible for most industrial gas–liquid flows, several authors (Sokolichin and Eigen-

berger, 1994; Ranade, 1995; Pan et al., 2000) have used the Eulerian *k*-fluid model for simulation of the dynamic gas–liquid flow by modeling subgrid/local phenomena and simulating the large-scale phenomena. It is well known that the successful applications of such simulations in multiphase flow are mainly dependent on the appropriate closure laws for the interphase transport of mass, momentum, and energy (Delnoij et al., 1997; Kuipers and van Swaaij, 1998). For modeling multiphase flow in packed beds, additional effort is needed, as discussed earlier, to properly implement the porosity structure of packed beds into the model equations.

In this work, the computational fluid dynamics code, CFDLIB, developed by the Los Alamos National Laboratory (Kashiwa et al., 1994), has been adopted using a *k*-fluid model for the simulation of multiphase transient flows in packed beds. The key aspects of the *k*-fluid model and the main features of CFDLIB code are described below.

k-Fluid equations and solution in CFDLIB

CFDLIB is a library of hydrocodes that share a common numerical solution algorithm, and a common data format (i.e., "block-structured"). There is a hierarchy to the codes in CFDLIB, which depends on the complexity of the systems dealt with (from multispecies, multiphase, and compressible system to single species, single phase, and incompressible system). The time-dependent mass, momentum, and energy conservation equations were derived using the ensemble-averaging technique, were cast in the integral form, and the solution was based on the finite-volume method (FVM) (Kashiwa et al., 1994).

In the finite-volume approach, the physical domain is subdivided into small volumes, and the dependent variables are evaluated either at the center of the volumes (cells) or at the corners (vertices) of the volumes. In the CFDLIB codes, the physical domain is divided into the main computational subunits: *blocks*, *sections*, and *cells*. A *block* is a logical rectangular portion of the meshes, having left, right, bottom, and top boundaries. In each mesh direction within the block there are several *sections*. In each section, the material data are constant and are specified in the input file before initializing the calculation. Therefore, the material data distribution information can be introduced into the computational domain through each section. Moreover, the code allows unequal section size within a single block. All these features allow inputting detailed porosity distribution data as an initial condition in the input file. The code can discretize each section into *cells*; each *cell* has four vertices and four faces for the 2-D simulation treated here. Each interior face is common to two cells, and each interior vertex is common to four cells. Figure 2 illustrates how to assign the logical block, sections, and cells from the physical block in the 2-D CFDLIB code, respectively. It is noted that in the 2-D CFD computation in CFDLIB code, the 2-D cells still represent 3-D volumes. For example, in a 2-D Cartesian coordinate, the cells have a nominal depth of $\Delta z = 1$ length unit.

For the system with more complicated geometry, several blocks are needed, which can be linked together in logical space by boundaries that are completely transparent to the flow (Johnson et al., 1997). The finite-volume method used in CFDLIB has an obvious advantage over a finite difference

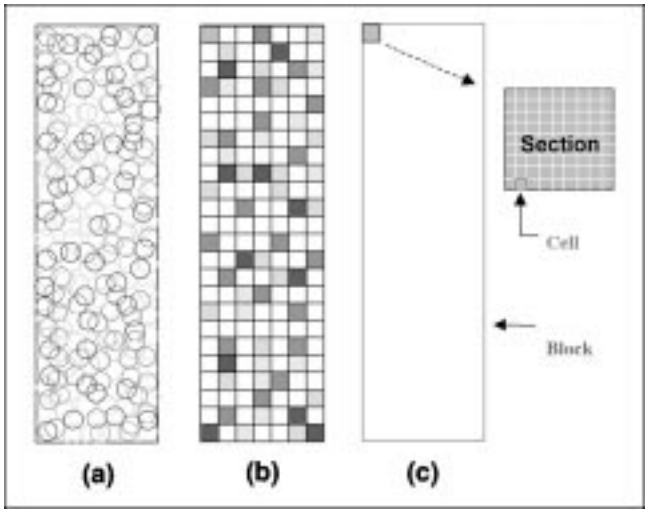

Figure 2. Block, sections, and cells in CFDLIB for packed-bed modeling.

(a) Physical block, that is, actual bed to be modeled; (b) sectional representation of the bed (porosity value is constant within a section); (c) cells or meshes in the sections (cell representation for computational purposes, all the cells within one section have the same porosity).

method if the physical domain is highly irregular and complicated, since arbitrary volumes can be utilized to subdivide the physical domain. Since the integral equations are solved directly in the physical domain, no coordinate transformation is required. Also the mass, momentum, and energy are automatically conserved, since the integral forms of the governing equations are solved (Tannehill et al., 1997).

The ensemble-averaged conservation equations that serve as the basis for *k*-fluid model in CFDLIB are the continuity and momentum equations. The continuity equation is

$$\frac{\partial \rho_k}{\partial t} + \nabla \cdot \rho_k \bar{u}_k = < \rho_0 \dot{\alpha}_k > \qquad (1)$$

The terms on the lefthand side of Eq. 1 constitute the rate of change in mass of phase k at a given point, and the term on the righthand side is the source term due to transport of mass from one phase to the other. Here, α_k represents the net rate at which material k is being created. In the present study this term is equal to zero since no phase exchange, reaction, or mass transfer is considered at this stage.

The momentum equation is given by:

$$\frac{\partial \rho_k \bar{u}_k}{\partial t} + \nabla \cdot \rho_k \bar{u}_k \bar{u}_k = + < \rho_0 \dot{\alpha}_k \bar{u}_o > \quad \text{(mass exchange source)}$$

$$- \nabla \cdot < \alpha_k \rho_0 \underline{u}'_k \underline{u}'_k > \quad \text{(Reynolds stress)}$$

$$- \theta_k \nabla p \quad \text{(equilibration pressure)}$$

$$- \nabla \theta_k \left(p_0^k - p \right) \quad \text{(nonequilibrium pressure)}$$

$$- < \left[-(p_0 - p)\bar{\bar{I}} + \bar{\bar{\tau}}_0 \right] \cdot \nabla \alpha_k > \quad \text{(momentum exchange)}$$

$$+ \nabla \cdot < \alpha_k \bar{\bar{\tau}}_0 > \quad \text{(average stress)}$$

$$+ \rho_k \bar{g} \quad \text{(body force)}. \quad (2)$$

To close Eq. 2, the closure models for computing the Reynolds stress and the momentum exchange terms are needed. Such closure problems can be resolved either by phenomenological models (e.g., Ergun equation), or by the formula from the microstructure flow element (e.g., DNS), or from an original transport equation (e.g., lattice Boltzmann simulation). In the flow modeling of packed beds discussed in this article, the phenomenological closure formulas based on experimental data are used.

CFD Modeling Issues Specific to Packed Beds

To adopt the CFDLIB code to the present flow problem in packed beds some subroutines related to the closures and phase-pressure calculations need to be added and modified to carefully take into account the essential physics of the system.

Significance of terms in the momentum balance

To numerically describe the flow pattern at different scales, one has to formulate the governing flow equations with different basic force terms: inertial force, viscous force, capillary force, gravitational force, turbulence-related force, and so on. For example, one has to take the Reynolds stress term into consideration in the fine-mesh CFD modeling with high gas flow rate (Logtenberg and Dixon, 1998). In fact, the existence of microscale turbulence in porous media has been detected by several experiments by pointwise probes (Jolls and Hanratty, 1966; Latifi et al., 1989). For the macroscopic flow modeling in packed beds, however, the contribution of the Reynolds stress term to the fluid momentum equation is not important (Jiang et al., 2000) because the microscopic turbulence is smoothed out when averaging a number of local (random) signals within a representative elementary volume (such as a cubic cell contains a cluster of particles). More discussions of micro- and macroscale turbulence modeling in porous media are available elsewhere (Lage, 1998).

The size and the shape of the packing elements determine the void structure of the granular assembly, which further affects the contribution of each basic force on the flow distribution. Table 1 lists the typical ranges of the ratio of forces in gas and liquid flow through the packed granules. Obviously, oil displacements are capillary-dominated creeping flows. In packed beds used as separation columns with large packing elements (e.g., 10 ∽ 30-mm Pall rings and Raschig rings), both the gravity and inertial forces are important, whereas the liquid distribution patterns are not very sensitive to the wetability of the packing surface (see Bemer and Zuiderweg, 1978) due to the negligible capillary force. However, in trickle beds, the particle sizes are typically in the range of 0.5 to 3 mm, and all the forces contribute to the flow distribution, and the influence of particle external wetting on liquid distribution can be significant (Lutran et al., 1991; Ravindra, et al., 1997; Jiang et al., 1999). This implies that even for describing the same macroscale flow pattern in the whole packed bed, the contribution of each basic-force may be of different magnitude, depending on the different characteristic radii of the flow passages.

The inertial effect on flow in porous media has been the topic of debate for many years (Stanek, 1994; Lage, 1998). The numerical modeling of single-phase flow in packed beds has shown that the contribution of the inertial term to the total (mechanical) energy dissipation rate is negligible compared to the viscous term and to the kinetic term, *except* in the regions of structural obstacles that change the flow direction sharply (Jiang et al., 2000). This agrees with the experimental findings of gas flow through the packed beds with obstacles (Choudhary et al., 1976). In trickle beds with two-phase cocurrent flow, the increase in gas and liquid flow rates can generate high inertial forces exerted in the bulk fluids, which further contributes to the growth of interfacial waves and to the bed-scale destabilization of the trickle-flow regime. On the other hand, the high inertial force causes gradients in liquid saturation, and results in the capillary force at gas and liquid interface, which contributes to the attenuation of interfacial waves and to the stabilization of the trickle-flow regime. The simulation of 1-D bed using a *k*-fluid model has shown that the inertial forces play an important role in the mechanism of flow transition from trickling to pulsing flow (Grosser et al., 1988; Attou and Ferschneider, 2000).

In summary, the Reynolds stress term is not important in determining the macroscale flow pattern in packed beds with a particle size of 10^{-4} to 10^{-2} m; however, other basic forces (i.e., inertial, viscous, gravity, and capillary forces) are normally of a similar order of magnitude so that they have to be taken into account in the flow equations in a proper way.

Closures for multiphase flow equations

The volume-averaging technique for equations of motion leads to the well-known closure issue for some of the terms

Table 1. Typical Ranges of the Ratio of Forces in Two-Phase Flow in Granular Packing

Packings	Particle d_p, m	*Re* Inertial/Viscous	*Ca* Viscous/Capillarity	1/*Bo* Capillarity/Gravity
Porous media: oil displacement; chromatography	10^{-7}–10^{-4}	10^{-9}–10^{-2}	10^{-7}–10^{-3}	10^{2}–10^{9}
Trickle beds	10^{-3}–10^{-2}	10^{-2}–10^{3}	10^{-1}–10	10^{-1}–10
Separation cloumns	10^{-2}–10^{-1}	10–10^{5}	10–10^{2}	10^{-3}–10^{-1}

Reynolds number: $Re_p \equiv \rho d_p U_k / \mu_k$; capillary number: $Ca \equiv \mu_L U_L / \sigma_S$; bond number: $Bo \equiv [d_p^2 (\rho_L - \rho_G) g] / \sigma_S$

Source: Adapted from Melli et al., 1990.

associated with fluctuating variables and source terms in which some of the forces acting on a representative permeable volume need to be modeled. For single-phase flow through porous media, several studies used the effective viscosity idea of Brinkman, and lumped the forces acting on the fluid phase of the permeable medium into an effective viscous force (Bey and Eigenberger, 1997). In this work, we compute the drag forces due to fluid–particle and fluid–fluid interactions based on the phenomenological models developed in bench-scale hydrodynamic experiments. Moreover, the magnitude of the drag force is expressed as a product of a user-defined exchange coefficient, X_{kl}, phase volume fractions, θ_l, θ_k, and relative interstitial velocity of the two phases k and l as below

$$F_{D(k-l)} = - < \left[-(p_0 - p)\bar{\bar{I}} + \bar{\bar{\tau}}_0 \right] \cdot \nabla \alpha_k = \theta_k \theta_l X_{kl}(u_k - u_l). \tag{3}$$

Clearly, in order to use Eq. 3, it is essential to determine the values of the exchange coefficient, X_{kl}.

Thus far, there are several models capable of providing X_{kl} values, namely, the relative permeability model (Saez and Carbonell, 1985), the single-slit model (Holub et al., 1992), the two-fluid interaction model (Attou et al., 1999) (see Eqs. 4 through 8 as tabulated in Table 2). Note that the interaction force between the gas and the liquid phase was neglected in both the single-slit and relative-permeability models, indicating zero shear stress at the gas–liquid interface. This may be true only for the case where gas and liquid flow rates are both small, and the flow system is located "deep" in the trickling flow regime. Otherwise, one does need to take into account this force in the hydrodynamic computations, because experimental studies of Larachi et al. (1991) and Al-Dahhan and Dudukovic (1994) have shown that gas flow can exert considerable influence on the hydrodynamics of the trickle-bed reactor, especially at high operating pressure and/or high gas velocity. Hence, Attou et al. (1999) included the gas–liquid interaction force (see Eq. 8 in Table 2) in the 1-D two-fluid model based on an "annular-flow" model, in which the gas and liquid phases are separated by a smooth and stable interface. Good predictions of liquid holdup and pressure drop were claimed in this article. In our earlier CFD simulations of two-phase flow (Jiang et al., 1999), either no interaction was assumed or a drag formula for a single sphere in fluid was used as an approximation for the momentum gas–liquid exchange coefficient, X_{gl}. In this work, the gas–liquid interfacial drag formula for X_{gl} developed by Attou et al. (1999) has been chosen due to its more appropriate physical basis.

Since the difference in the topology of the pore structure may exist from bed to bed even for beds with the same mean porosity, the use of Ergun constants (E_1 and E_2) determined in a bed of interest from single-phase flow experiments were

Table 2. Models for Drag Coefficients

Single-slit model (Holub et al., 1992)

Fluid–particle: (X_{ls} and X_{gs})

$$X_{ks} = (A_{ks}\mu_k U_k + B_{ks}\rho_\alpha U_k^2)\frac{1}{(1-\epsilon)|u_k|} \tag{4}$$

$$A_{ks} = E_1\frac{(1-\epsilon)^2}{\vartheta_k^3 d_p^2}; \quad B_{ks} = E_2\frac{(1-\epsilon)}{\vartheta_k^3 d_p}$$

Relative permeability model (Saez and Carbonell, 1985)

Fluid–particle: (X_{ls} and X_{gs})

$$X_{ks} = (A_{ks}\mu_k U_k + B_{ks}\rho_\alpha U_k^2)\frac{1}{(1-\epsilon)|u_k|} \tag{5}$$

$$A_{gs} = 180\frac{(1-\epsilon)^2\epsilon^{1.8}}{\vartheta_g^{4.8} d_p^2}; \quad B_{gs} = 1.8\frac{(1-\epsilon)\epsilon^{1.8}}{\vartheta_g^{4.8} d_p}$$

$$A_{ls} = 180\frac{(1-\epsilon)^2}{\vartheta_l^3 d_p^2}\left(\frac{\epsilon-\theta_l^0}{\theta_l-\theta_l^0}\right)^{2.43}; \quad B_{ls} = 1.8\frac{(1-\epsilon)}{\vartheta_l^3 d_p}\left(\frac{\epsilon-\theta_l^0}{\theta_l-\theta_l^0}\right)^{2.43}$$

Two-fluid intreraction model (Attou et al., 1999)

Fluid–particle: (X_{ls} and X_{gs})

$$X_{ls} = (A_{ls}\mu_l U_l + B_{ls}\rho_l U_l^2)\frac{1}{(1-\epsilon)|u_l|} \tag{6}$$

$$A_{ls} = 180\frac{(1-\epsilon)^2}{\vartheta_l^3 d_p^2}; \quad B_{ls} = 1.8\frac{(1-\epsilon)}{\vartheta_l^3 d_p}$$

$$X_{gs} = \frac{\theta_g}{\epsilon}(A_{gs}\mu_g U_g + B_{gs}\rho_g U_g^2)\frac{1}{(1-\epsilon)|u_g|} \tag{7}$$

$$A_{gs} = 180\frac{(1-\theta_g)^2}{\vartheta_g^3 d_p^2}\left(\frac{1-\epsilon}{1-\theta_g}\right)^{2/3}; \quad B_{gs} = 1.8\frac{(1-\theta_g)}{\vartheta_g^3 d_p}\left(\frac{1-\epsilon}{1-\theta_g}\right)^{1/3}$$

Fluid–fluid: (X_{gl})

$$X_{gl} = \frac{\theta_g}{\epsilon}(A_{gl}\mu_g U_r + B_{gl}\rho_g U_r^2)\frac{1}{\theta_l|u_g-u_l|} \tag{8}$$

$$A_{gl} = A_{gs}; \quad B_{gl} = B_{gs}; \quad U_r = \theta_g|u_g - u_l|$$

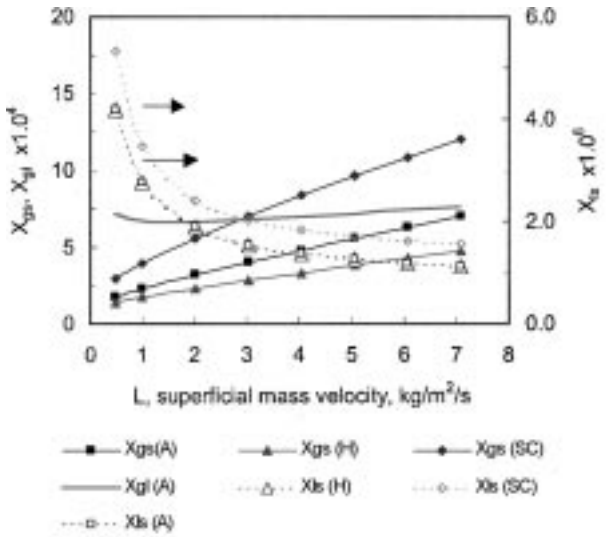

Figure 3. Comparison of drag coefficient X_{kl} (X_{gs}, X_{ls}, and X_{gl}), from different models.

A—Two-fluid interaction model (Attou et al., 1999); H—single-slit model (Holub et al., 1992); SC—relative permeability model (Saez and Carbonell, 1985).

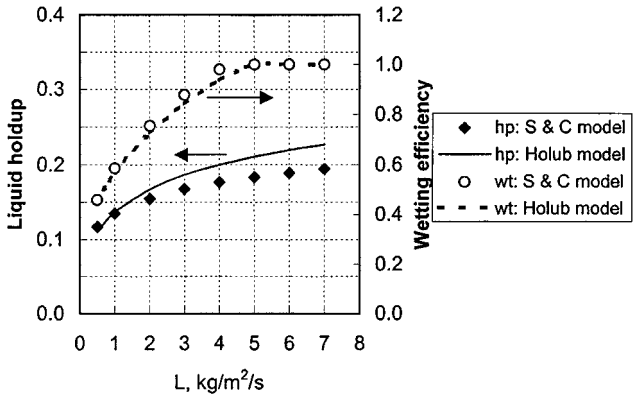

Figure 4. Effect of liquid superficial mass velocity on liquid holdup (hp) and particle external wetting efficiency (wt) at a gas superficial velocity of 6 cm/s.

Holub model (single-slit model; see Holub et al., 1992); S & C model (relative permeability model; see Saez and Carbonell, 1985). Particle external wetting efficiency values (wt) were calculated by the correlation of Al-Dahhan and Dudukovic (1995). wt-S & C model means that the pressure-drop value used in calculating the wt value was from the S & C model; wt-Holub model means the pressure-drop value used in calculating the wt value was from Holub's model.

suggested in the single-slit model to obtain better predictions for liquid holdup and pressure drop in two-phase flow (Holub et al., 1992). However, in the relative permeability model (Saez and Carbonell, 1985) and in the two-fluid interaction model (Attou et al., 1999), the values 180 and 1.8 were used for E_1 and E_2, respectively, as recommended by McDonald et al. (1979). As a remedy, the choice of the permeability function and of the static liquid holdup, ϵ_L^0, in the relative permeability model allow for additional consideration of the porosity topology to some extent. Only the two-fluid interaction model of Attou et al. (1999) has no adjustable parameters in the calculations of liquid holdup and pressure drop. For multiphase flow simulation discussed in this work, since the structural characteristics of the packed bed have been introduced into the flow equations through the sectional porosity distribution, the use of fixed values of E_1 and E_2 are appropriate. However, instead of using the universal Ergun constant values of 150 and 1.75 used in single-phase flow simulation (Jiang et al., 2000), for the multiphase flow case the values of 180 and 1.8 are suggested.

The expressions for the other two-phase momentum exchange coefficients, X_{kl}, are written in similar format in Table 2. The comparisons of these expressions for the given sectional porosity and particle size are shown in Figure 3. For a given gas superficial velocity of 6.0 cm/s, an increase in liquid mass superficial velocity causes X_{gs} to increase and X_{ls} to decrease. Moreover, the relative permeability model gives relatively higher values of X_{gs} and X_{ls} than either the single-slit model or the two-fluid interaction model. Hence, the relative-permeability model gives lower predictions of liquid holdup than the single-slit model at the same flow conditions, as shown in Figure 4. The two-fluid interaction model yields the same values of X_{ls} as the slit model, and provides intermediate values of X_{gs}, between the slit model and the relative-permeability model. The effect of liquid superficial mass velocity on the X_{gl} value is not significant. Due to the lack of detailed flow velocity and volume-fraction distribution data together with the known bed structure at certain section sizes, we are not able to establish the best drag expression for X_{gl} at the present time. However, we can illustrate how these drag expressions affect the predictions of the liquid holdup and pressure gradient at the bed scale, as shown in Part II (Jiang et al., 2002). The full validation of the best drag expression, in principle, should be possible by using the MRI technique to obtain the needed experimental data.

The overall external particle wetting efficiency can be calculated by the correlation of Al-Dahhan and Dudukovic (1995) based on the local superficial velocities of gas and liquid as well as particle parameters and so forth. As shown in Figure 4, at the bed scale, the external particle partial wetting does exist at a low liquid superficial mass velocity ($L < 5.0$ kg/m^2/s). Therefore, the drag formulations derived from the double-slit model, in which two interconnected slits—wet and dry slit—are assumed (see Iliuta et al., 2000), could provide a reasonable alternative, because then it is possible to account for particle wetting in the multiphase drag calculations. However, the computation becomes more cumbersome due to the numerous equations involved in the double-slit model. Furthermore, how much improvement can be gained is still uncertain, because the comparison of predictions of various models with global hydrodynamics quantities led Larachi et al. (2000) and Iliuta et al. (2000) to conclude that all of these models fit the experimental data to about the same degree of accuracy.

Interfacial-tension effect, wetting correction

Direct and indirect liquid flow visualizations have shown that the effect of prewetting of the packing on liquid distribution is significant (Lutran et al., 1991; Ravindra, et al., 1997;

Jiang et al., 1999). The analysis of the basic forces outlined in the subsection on the significance of terms in the momentum balance also confirms this result. In general, liquid holdup and particle wetting efficiency are reduced, and liquid rivulets are favorably formed when introducing trickle flow into the dry packing. Moreover, the liquid distribution in packed beds is a function of flow history (Lutran et al., 1991; Ravindra et al., 1997). It means that the wetting state of the particle surface significantly affects the flow distribution. Experimental studies have established that the gas and liquid interfacial tension forces and the packing wettability are not only responsible for the liquid flow maldistribution (see Lutran et al., 1991), but are also responsible for the hysteresis observed in the pressure drops and liquid holdup measured during cocurrent and countercurrent flow in packed beds (see Levec et al., 1988). To numerically capture these flow phenomena, one must consider the interfacial tension effect and packing wettability in the pressure calculations.

When two immiscible fluids (such as gas and liquid) are in contact with each other, interfacial tension causes the fluids to have different pressures. This discontinuity in pressure between fluids is known as the capillary pressure, P_c. Specifically, we define the capillary pressure between gas (G) and liquid (L) as

$$P_G - P_L = P_c \tag{9}$$

At a pore scale the capillary pressure can be expressed by

$$P_c = 2\sigma_S\left(\frac{1}{d_1} + \frac{1}{d_2}\right) \tag{10}$$

The characteristic lengths d_1 and d_2 are further described in terms of particle diameter, local porosity, and the minimum equivalent diameter of the area between three particles in contact, as well as pressure factor, F, as given in Attou and Ferschneider (2000)

$$P_c = 2\sigma_S\left(\frac{\theta_S}{1-\theta_G}\right)^{1/3}\left(\frac{1}{d_p} + \frac{1}{d_{\min}}\right)F\left(\frac{\rho_G}{\rho_L}\right) \tag{11}$$

The capillary pressure could also be expressed through the permeability concept together with the correlation of the experimental data in various porous media. Grosser et al. (1988) proposed the following expression for calculating the capillary pressure:

$$P_c = \sigma J(\theta_L, \theta_S)\left(\frac{1-\theta_S}{k}\right)^{0.5} \tag{12}$$

where σ is the surface tension; θ_L and θ_S are liquid and solid phase volume fraction, respectively; k is the permeability of the porous media, which is related by Eq. 13 to the Ergun constant (E_1) and the equivalent particle diameter (d_e) for viscous flow in packed beds; J is a dimensionless function obtained from the experimental data taken on various sand samples with air and water (Leverett, 1941), as given by Eq. 14

$$\left(\frac{1-\theta_S}{k}\right)^{0.5} = \frac{\theta_S E_1^{0.5}}{(1-\theta_S)d_e} \tag{13}$$

$$J(\theta_L, \theta_S) = 0.48 + 0.036\ln\left(\frac{1-\theta_S-\theta_L}{\theta_L}\right) \tag{14}$$

Therefore, the capillary pressure is a function of liquid holdup, and the gradient of the capillary pressure depends on the gradient of liquid holdup in the packed bed. From the experimental observation of liquid distribution in prewetted and non-prewetted beds (see Jiang, 2000), complete prewetting of the particle surface can greatly reduce the gradient of liquid holdup in the packed bed, which considerably reduces the capillary pressure effect on liquid distribution. For the modeling of macroscale flow, Eq. 9 is further modified by incorporating the particle wetting factor, f, or external particle wetting efficiency (a fraction of external particle area wetted by liquid), as given below

$$P_L = P_G - (1-f)P_c \tag{15}$$

By substituting Eqs. 11, or Eqs. 12, 13, and 14, into Eq. 15, one gets Eqs. 16a and 16b, respectively:

$$P_L = P_G - 2\sigma_S(1-f)\left(\frac{\theta_S}{1-\theta_G}\right)^{1/3}\left(\frac{1}{d_p} + \frac{1}{d_{\min}}\right)F\left(\frac{\rho_G}{\rho_L}\right) \tag{16a}$$

$$P_L = P_G - (1-f)\sigma_S\frac{\theta_S E_1^{0.5}}{(1-\theta_S)d_e} \times\left[0.48 + 0.036\ln\left(\frac{1-\theta_S-\theta_L}{\theta_L}\right)\right] \tag{16b}$$

This indicates that the macroscale capillary effect is negligible when the particles are completely externally wetted ($f = 1.0$), whereas this effect is most significant when the particle surfaces are completely dry ($f = 0$), as evidenced from the experimental results with the nonprewetted beds (Jiang et al., 1999).

In the CFD flow simulation the value of the particle wetting factor at each cell scale can be evaluated based on the local cell scale flow velocities and local pressure gradient using the correlation of Al-Dahhan and Dudukovic (1995) for the external wetting efficiency of particles in small trickle beds

$$f = 1.104\left(\frac{Re_L}{1-\epsilon}\right)^{1/3}\left[\frac{\frac{\Delta P}{\rho_L g Z} + 1}{Ga_L}\right]^{1/9} \tag{17}$$

The simulations reveal that in cases of partial particle wetting ($f < 1.0$), the contribution of the macroscale capillary

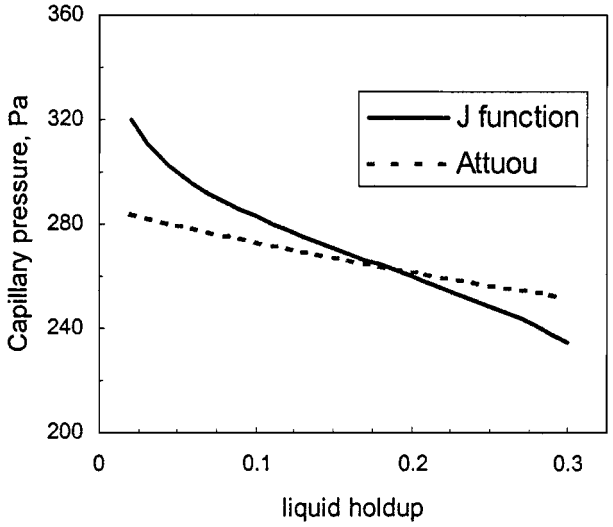

Figure 5. Comparison of the calculated capillary-pressure values from two different expressions, Eqs. 16a and 16b, for air–water system.

$d_p = 0.003$ m; $\theta_s = 0.63$.

pressure on liquid flow distribution is significant. It is thus expected that the hysteresis observed in the pressure drops and global liquid holdup at bed scale is due to the hysteresis in liquid flow distribution. This in turn is caused by the capillary pressure hysteresis and different particle wetting status in liquid imbibition and drainage experiments.

There is a difference in the capillary-pressure values calculated by Eqs. 16a and 16b, even for the same system of air–water as shown in Figure 5. It is noted that Eq. 16b was originally derived exclusively based on the experimental data for air–water flow through consolidated porous media (such as sands, Leverett, 1941). This expression was suggested for flow through packed beds by Grosser et al. (1988) without experimental confirmation. The derivation of Eq. 16a was based on the local linear momentum balance law, applied to the gas–liquid interface, in which the effect of gas density was incorporated through $F(\rho_G/\rho_L)$, and was claimed to be suitable for elevated pressure systems (see Attou and Ferschneider, 2000). In fact, there have been no direct experiments designed for validation of these two expressions for trickle beds, although the measurement of capillary rise in packed beds by Kramer (1998) may provide some assistance for such experiment design to discriminate between the two capillary pressure models. For the present, the *J*-function expression (i.e., Eq. 16b) is used for the air–water system, and the expression of Attou and Ferschneider (2000) can be used for other systems, particularly at elevated operating pressures.

Effect of mesh size on computed results

In general, a chosen grid is used for a discrete representation of the continuous-field phenomena that one wants to model. The accuracy and numerical stability of the simulation depends on the choice of the grid (Tannehill et al., 1997). In the CFDLIB code the finite-volume method is used to discretize the conservation equations. At this stage, we utilized two different 2-D coordinate systems for generation of the grid cells: the Cartesian and cylindrical coordinates. In the 2-D cylindrical coordinates, we assume that there is no dependence on the θ-direction. Although the flow in a cylindrical column does distribute in three dimensions, the radial and vertical distributions of the flow often play a more important role than the θ-direction distribution in determining the reactor performance (Stanek, 1994). In addition to discretization in space, an explicit temporal discretization scheme is utilized in the code, so the solution proceeds with respect to a sequence of discrete time, t^n, where n is the cycle number ($n = 0, 1, 2, \ldots$). The time step $\Delta t^n = t^{n+1} - t^n$ varies from cycle to cycle.

As discussed in the third section, there exists a relationship between the section size and the standard deviation of sectional porosities (such as Gaussian p.d.f.). After the section size is chosen, the porosity distribution is specified so as to assign a single value of porosity to every given section. The

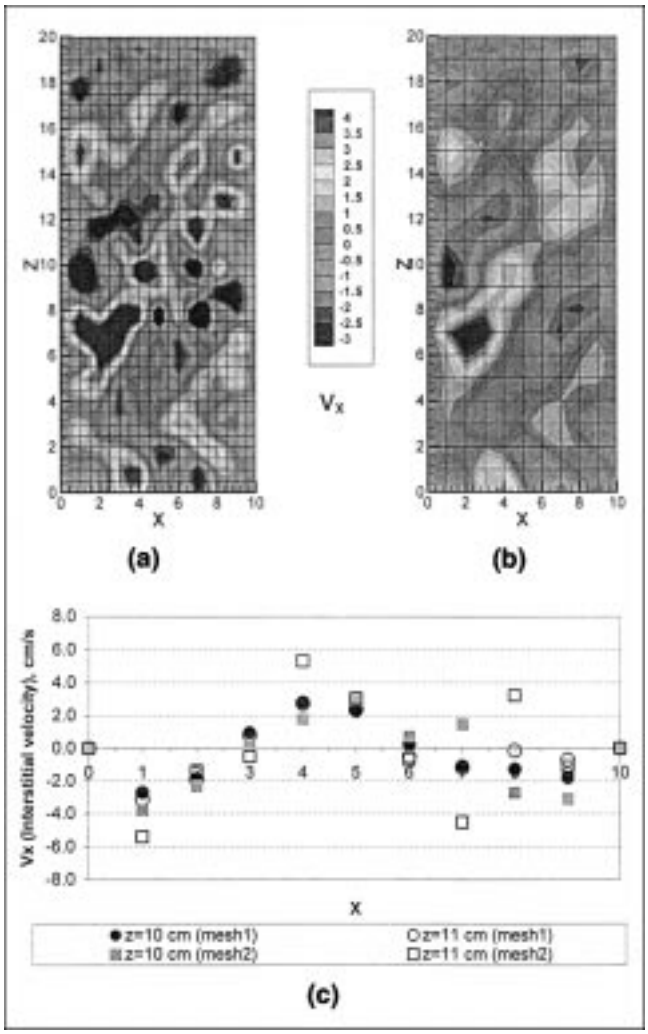

Figure 6. Simulated liquid-upflow horizontal-velocity component, V_x, contours.

It uses (a) mesh2 (10×20 sections, 20×40 cells; mesh size = 0.5 cm); (b) mesh1 (10×20 sections, mesh size = 1.0 cm) at a superficial velocity of 10 cm/s; and (c) horizontal profile of the horizontal-velocity component.

computational cell size is then specified, equal to or smaller than section size. Each cell within a section is assigned the same porosity of that section. Once a converged solution has been obtained, it is essential to assess the invariance of the computed results with respect to the section discretization. Particularly for the flow in packed beds, various flow scales and structural scales exist that make the selection of the grid size important for generating meaningful computational results. To test the dependence of the solution on the grid size, two simulations, one with a coarse grid (mesh1), and another with fine grid size (mesh2) were performed. Figures 6 and 7 show the comparison of the steady-state liquid upflow interstitial velocity components (V_x, V_z) in the forms of contour- and transversal-velocity profiles. Apparently, the flow patterns do not significantly vary when the cell size is changed from 1.0 cm to 0.5 cm. However, more detailed flow characteristics are obtained in the fine-cell simulation (mesh2). Figure 8 shows the initial solid volume fraction at a section size of 1 cm for two-phase cocurrent downflow simulation at the gas and liquid superficial velocities of 0.001 m/s and 0.05 m/s, respectively. If one zooms in on a specific square area, $x = 0 \sim 4$, and $z = 4 \sim 8$, one can see that the sectional flow patterns are similar, but the cell scale flow texture becomes more detailed when the computational cell size is reduced from 1.0 cm (mesh-a) to 0.5 cm (mesh-b) and to 0.25 cm (mesh-c), as shown in Figure 9. In Figure 10, we plot the calculated gas holdup profiles at a specific axial position ($x = 0 \sim 4$; $z = 8$), as marked in Figure 8, using three different mesh sizes (a, b, and c). No significant variation in gas holdup predictions was found.

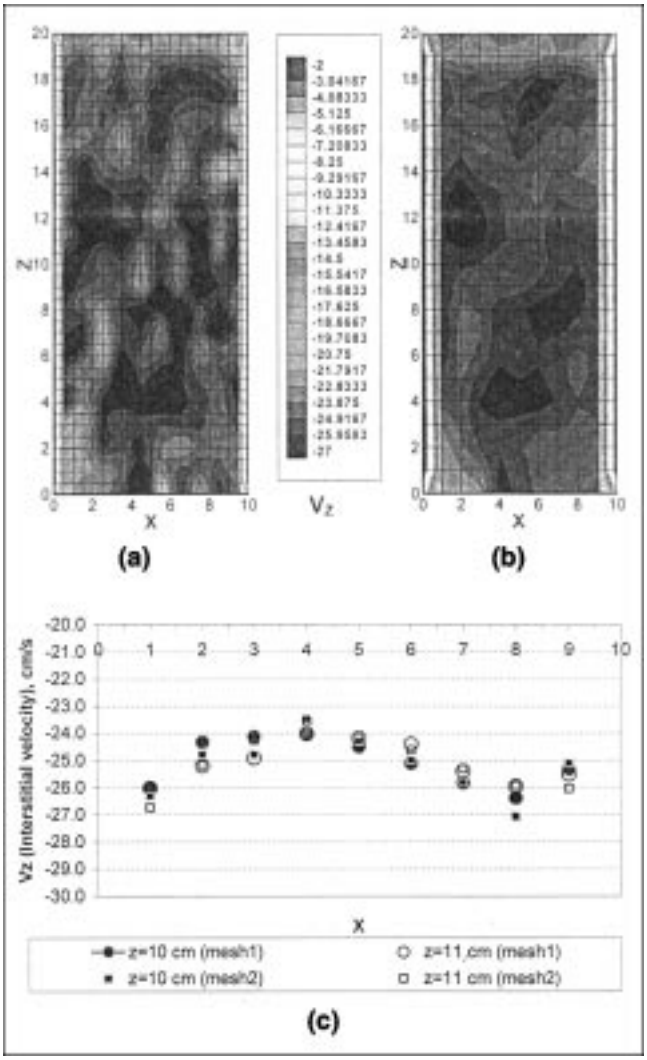

Figure 7. Simulated liquid-upflow vertical-velocity component, V_z, contours.

It uses (a) mesh2 (10×20 sections, 20×40 cells; mesh size = 0.5 cm); (b) mesh1 (10×20 sections, mesh size = 1.0 cm) at a superficial velocity of 10 cm/s; and (c) horizontal profile of the vertical-velocity component.

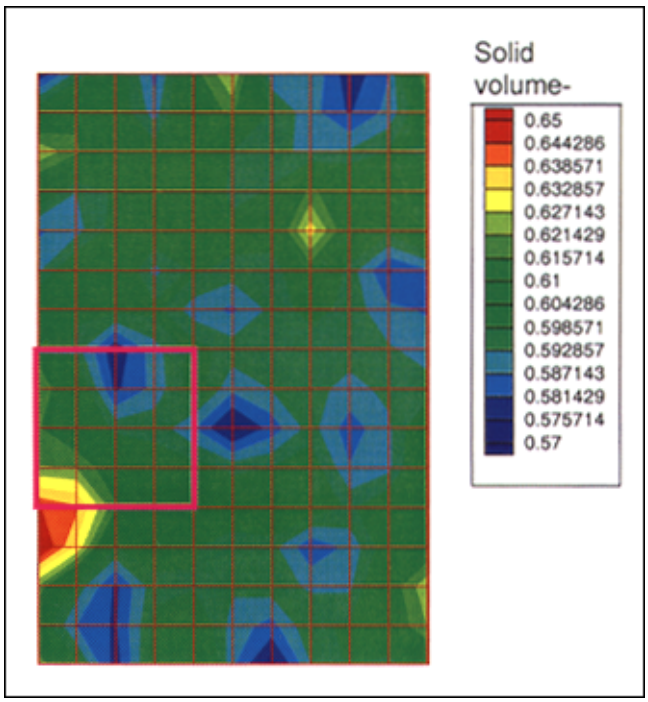

Figure 8. Initial solid volume fraction distribution at 10 ×15 section discretization (section size = 1.0 cm) for gas–liquid cocurrent downflow simulation.

The marked zone ($x = 0 \sim 4$; $z = 4 \sim 8$) consists of 16 sections.

Boundary conditions

It is well known that the quality of flow distribution at the top boundary can have a profound influence on the bed dynamics (Christensen et al., 1986). Szady and Sundaresan (1991) experimentally examined the effects of the top boundary and the bottom boundary on the hydrodynamics in a pilot-scale trickle bed. They found that both the top and bottom boundaries affect the flow characteristics in the trickling regime of flow, such as overall pressure gradient and liquid saturation. They also affect the onset of pulsing. In the flow simulations of interest in this work, special care has been taken in setting all boundary conditions. The stationary boundary conditions are used in most flow simulations with steady-state feed conditions in packed beds. This includes specified inflow velocities of fluids, zero velocity-gradient for

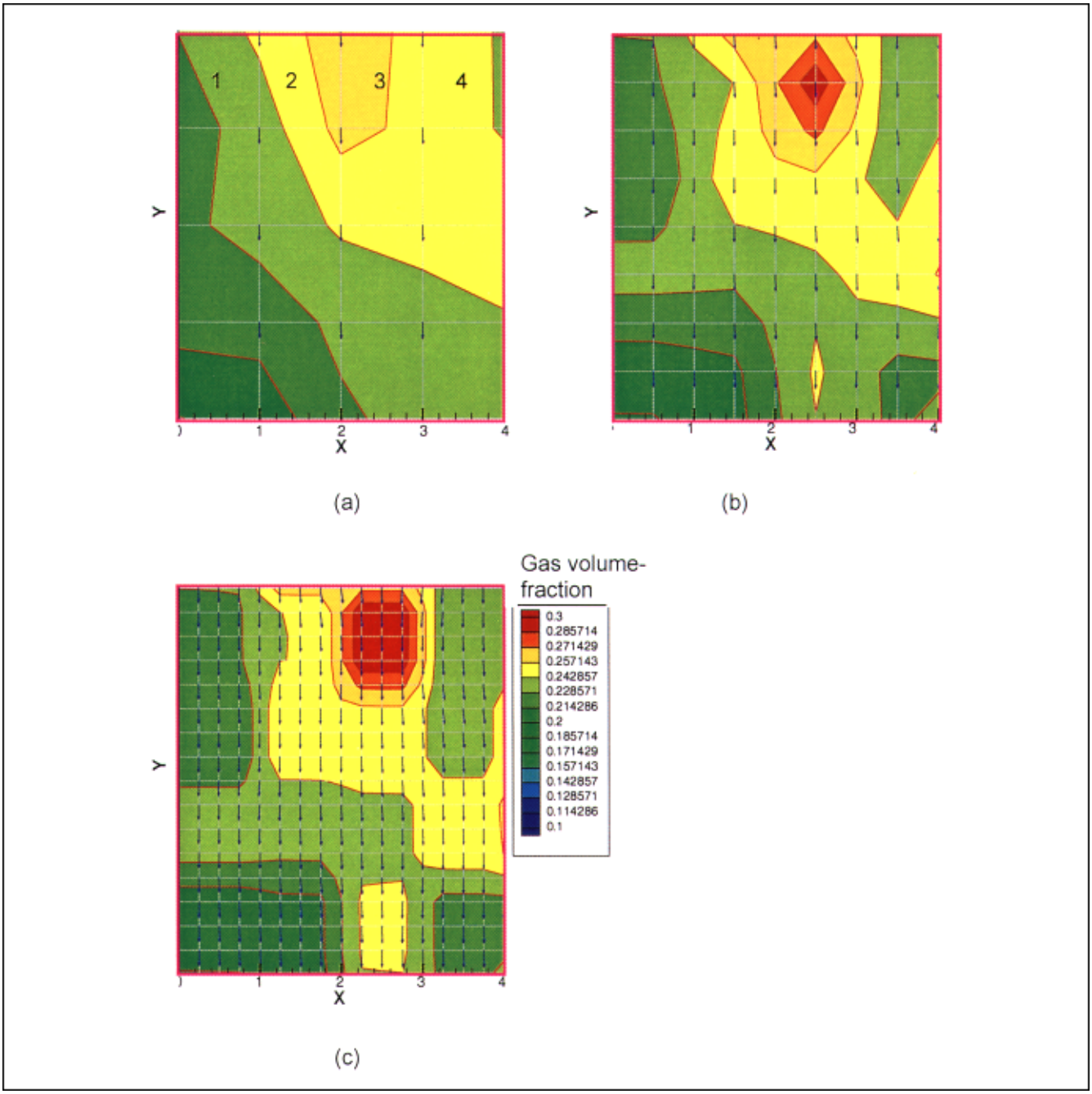

Figure 9. Gas-phase holdup contours and gas interstitial velocity vectors in the zone.

$x = 0 \sim 4$; $z = 4 \sim 8$ marked in Figure 8: (a) mesh-a: size = 1.0 cm; (b) mesh-b: size = 0.5 cm; (c) mesh-c: size = 0.25 cm.

the outflow, reflective boundary condition (or symmetry) at the center, and no-slip condition for the wall(s). However, for the case of the periodic liquid feed or gas feed case (so-called "on-off" flow modulation), the inflow velocity is specified to vary with time. For a 2-D cylindrical coordinates (a cylindrical bed), a reflective-wall boundary is used for the left side of the logical block (that is, the center line of the column); for a 2-D Cartesian coordinates (a rectangular bed), a no-slip condition wall is used for both the right and left side of the block. All the boundaries are treated as Eulerian boundaries since these boundaries are stationary in space even in the periodic operation. In Part II, we present the simulated flow distributions at both steady-state and unsteady-state flow feed conditions and show how the top boundaries affect the multiphase flow distributions in the entire packed bed.

Summary and Conclusions

The Eulerian *k*-fluid CFD model has been adopted to model the macroscale multiphase flow in packed beds in which the geometric complexity of bed structure is resolved

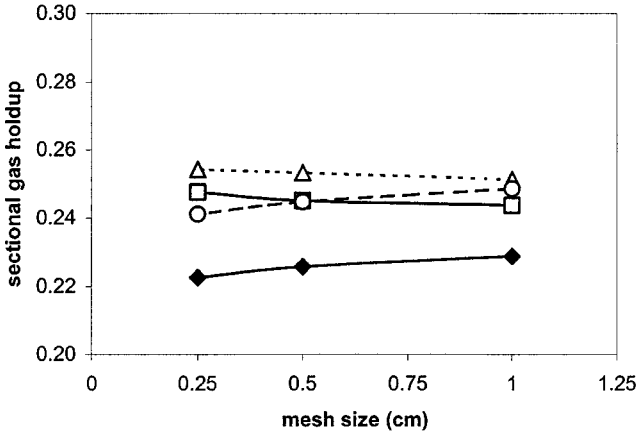

Figure 10. Effect of the mesh size on the comoputed sectional gas-holdup profiles.

Tracked the holdup values of four sections in the first row of 16 sections (Legend: Section 1: filled diamond; Section 2: square; Section 3: triangle; Section 4 circle).

through statistical implementation of sectional porosities, and the complicated multiphase interactions are evaluated using the Ergun type of expressions, which were developed based on bench-scale hydrodynamic experiments. The effect of particle wetting on flow distribution is incorporated in the phase-pressure computations. The drag formulas for fluid–particle and fluid–fluid interactions are examined and discussed. The drag-exchange coefficients for the solid particle and fluid, X_{ks}, are obtained based on the models of Holub et al. (1992) or Attou et al. (1999) with an E_1 of 180 and E_2 of 1.8. The drag-exchange coefficient for gas and liquid is calculated by the model of Attou et al. (1999). The *J*-function is used to calculate the capillary-pressure term. Due to the relationship between the section size and the variance of the sectional porosity, the selection of the section size has to follow a certain relation, which is expected to be available by analyzing the full 3-D porosity distribution data of MRI at fine spatial resolution (Sederman et al., 1997). The dependence of the simulated sectional-scale flow pattern on the cell size has been examined for both the liquid–solid and gas–liquid–solid systems, and it was demonstrated that a grid-independent macroscale flow structure is obtainable by the *k*-fluid CFD model, although the more detailed flow field may be apparent with a finer grid (i.e., small cell size).

Acknowledgment

We gratefully acknowledge the support of CREL industrial sponsors, which made this work possible, and thank the Los Alamos National Laboratory for providing the CFDLIB code. Special thanks are due to Dr. S. Kumar and Dr. S. Roy for valuable discussions of many CFD issues.

Notation

A_{gl}, A_{gs}, A_{ks} = parameters defined in Table 2
B_{gl}, B_{gs}, B_{ks} = parameters defined in Table 2
Bo = bond number
Ca = capillary number
D_r = diameter of packed bed, m
d_e = equivalent diameter of particle, m
d_p = particle diameter, m
$d_{\min}$ = minimum equivalent diameter of the area between three spheres in contact $\{d_{\min} = [(\sqrt{3}/\pi) - 0.5]^{0.5} d_p\}$, m
E_1, E_2 = Ergun constants ($E_1 = 180$; $E_2 = 1.8$)
f = particle wetting factor
F = pressure factor $[F(\rho_G/\rho_L) = 1 + 88.1(\rho_G/\rho_L)$ for $\rho_G/\rho_L < 0.025]$
$F_{D(k-l)}$ = drag between phases k and l
g = gravitational acceleration, 9.81 m/s^2
H = height of model bed, m
J = J function
k = relative permeability, m^2
L = superficial mass velocity, kg/m^2/s
l_s = size of section, m
n = time-step number
p = ensemble averaged pressure ($p \equiv \langle p_0 \rangle$), N/m^3
P_c = capillary pressure, N/m^3
P_G = pressure in gas phase, N/m^3
P_L = pressure in gas phase, N/m^3
p_0 = pressure, dyn/cm^2
p_0^k = pressure ($= < \alpha_k p_0 > / \theta_k$)
r = radial position in cylindrical coordinate, m
R = radius of packed beds, m
Re_p = Reynolds number, $V_0 d_p \rho/\mu$
S_k = saturation of phase k
t = time, s
u_0 = material velocity, m/s
$\bar{u}_k$ = material k interstitial velocity ($\rho_k u_k \equiv < \alpha_k \rho_0 u_0 >$), cm/s
$\bar{u}'_k$ = fluctuating part of material k interstitial velocity, m/s
U_0 = input superficial velocity ($= V_0 \times \epsilon_B$), m/s
V_G = gas interstitial velocity, m/s
V_L = liquid interstitial velocity, m/s
V_0 = input interstitial velocity ($= U_0/\epsilon_B$), m/s
$\vec{V}$ = velocity vector, m/s
X_{kl} = momentum exchange coefficient between phases k and l

Greek letters

α_k = material indicator ($=1$ if material k is present; $=0$ otherwise)
$\dot{\alpha}_k$ = material derivative
ϵ_B = mean porosity of packed bed
ϕ = particle shape factor, ($\phi = 1$ for Spherical particle)
μ = viscosity of fluid, Pa·s
θ_k = material k volume fraction ($\theta_k = < \alpha_k >$), k = G, L, S
θ_L^0 = static liquid holdup
τ_0 = deviatric stress
ρ = density of fluid, kg/m^3
ρ_k = density of material k ($\equiv < \alpha_k \rho_0 >$), g/cm^3
ρ_0 = material density, kg/m^3
σ_s = surface tension
σ_B = standard deviation of porosity distribution
$< >$ = ensemble average (e.g., $\langle Q_0 \rangle \equiv 1/N \sum_{r=1}^{N_R} Q_o(r)$, N_R is a large number
φ = angular coordinate

Literature Cited

Al-Dahhan, M. H., and M. P. Dudukovic, "Pressure Drop and Liquid Holdup in High Pressure Trickle-Bed Reactors," *Chem. Eng. Sci.*, **49**, 5681 (1994).

Al-Dahhan, M. H., and M. P. Dudukovic, "Catalyst Wetting Efficiency in Trickle-Bed Reactors at High Pressure," *Chem. Eng. Sci.*, **50**, 2377 (1995).

Anderson, T. B., and R. Jackson, "A Fluid Dynamical Description of Fluidized Beds," *Ind. Eng. Chem. Fundam.*, **6**, 527 (1967).

Anderson, D. H., and A. V. Sapre, "Trickle Bed Reactor Flow Simulation," *AIChE J.*, **37**, 377 (1991).
Attou, A., C. Boyer, and G. Ferschneider, "Modeling of the Hydrodynamics of the Cocurrent Gas-Liquid Trickle Flow through a Trickle-Bed Reactor," *Chem. Eng. Sci.*, **54**, 785 (1999).
Attou, A., and G. Ferschneider, "A Two-Fluid Hydrodynamic Model for the Transition between Trickle and Pulse Flow in a Cocurrent Gas-Liquid Packed-Bed Reactor," *Chem. Eng. Sci.*, **55**, 491 (2000).
Bemer, G. G., and F. J. Zuiderweg, "Radial Liquid Spread and Maldistribution in Packed Columns Under Different Wetting Conditions," *Chem. Eng. Sci.*, **33**, 1637 (1978).
Benenati, R. F., and C. B. Brosilow, "Void Fraction Distribution in Beds of Spheres," *AIChE J.*, **8**, 359 (1962).
Bey, O., and G. Eigenberger, "Fluid Flow Through Catalyst Filled Tubes," *Chem. Eng. Sci.*, **52**, 1365 (1997).
Chen, J., N. Rados, M. H. Al-Dahhan, M. P. Dudukovic, D. Nguyen, and K. Parimi, "Particle Motion in Packed/Ebullated Beds by CT and CARPT, *AIChE J.*, **47**, 994 (2001).
Choudhary, M., M. Propster, and J. Szekely, "On the Importance of the Inertial Terms in the Modeling of Flow Maldistribution in Packed Beds," *AIChE J.*, **22**, 600 (1976).
Christensen, G., S. J. McGovern, and S. Sundaresan, "Cocurrent Downflow of Air and Water in a Two-Dimensional Packed Columns," *AIChE J.*, **32**, 1677 (1986).
Crine, M., P. Marchot, and G. A. L'Homme, "Mathematical Modeling of the Liquid Trickling Flow Through a Packed Bed Using the Percolation Theory," *Comput. Chem. Eng.*, **3**, 515 (1979).
Crine, M., P. Marchot, and G. A. L'Homme, "Statistical Hydrodynamics in Trickle Flow Columns," *AIChE J.*, **38**, 136 (1992).
Cumberland, D. J., and R. J. Crawford, *The Packing of Particles*, Elsevier, New York (1987).
Delnoij, E., F. A. Lammers, J. A. M. Kuipers, and W. P. M. van Swaaij, "Dynamic Simulation of Dispersed Gas-Liquid Two-Phase Flow Using a Discrete Bubble Model," *Chem. Eng. Sci.*, **52**, 1429 (1997).
Drew, D. A., "Mathematical Modeling of Two-Phase Flow," *Annu. Rev. Fluid Mech.*, **15**, 261 (1983).
Dudukovic, M. P., F. Larachi, and P. L. Mills, "Multiphase Reactors: Revisited," *Chem. Eng. Sci.*, **54**, 1975 (1999).
Fox, R. O., "Computational Methods for Turbulent Reacting Flows in the Chemical Process Industry," *Rev. Inst. Fr. Pet.*, **51**, 215 (1996).
Grosser, K. A., R. G. Carbonell, and S. Sundaresan, "Onset of Pulsing in Two-Phase Cocurrent Downflow Through a Packed Bed," *AIChE J.*, **34**, 1850 (1988).
Holub, R. A., "Hydrodynamics of Trickle Bed Reactors," PhD Thesis, Washington Univ., St. Louis, MO (1990).
Holub, R. A., M. P. Dudukovic, and P. A. Ramachandran, "A Phenomenological Model for Pressure Drop, Liquid Holdup, and Flow Regime Transition in Gas-Liquid Trickle Flow," *Chem. Eng. Sci.*, **47**, 2343 (1992).
Iliuta, I., F. Larachi, and M. H. Al-Dahhan, "Double-Slit Model for Partially Wetted Trickle Flow Hydrodynamics," *AIChE J.*, **46**, 597 (2000).
Ishii, M., *Thermo-Fluid Dynamic Theory of Two-Phase Flow*, Eyrolles, Paris (1975).
Jiang, Y., M. R. Khadilkar, M. H. Al-Dahhan, and M. P. Dudukovic, "Two-Phase Flow Distribution in 2D Trickle-Bed Reactors," *Chem. Eng. Sci.*, **54**, 2409 (1999).
Jiang, Y., M. R. Khadilkar, M. H. Al-Dahhan, and M. P. Dudukovic, "Single Phase Flow Modeling in Packed Beds: Discrete Cell Approach Revisited," *Chem. Eng. Sci.*, **55**, 1829 (2000).
Jiang, Y., M. R. Khadilkar, M. H. Al-Dahhan, and M. P. Duduković, "CFD of Multiphase Flow in Packed-Bed Reactors: II. Results and Applications," *AIChE J.*, **48**(4), 716 (2002).
Jolls, K. R., and T. J. Hanratty, "Transition to Turbulence for Flow Through a Dumped Bed of Spheres," *Chem. Eng. Sci.*, **21**, 1185 (1966).
Johnson, N. L., B. A. Kashiwa, and W. B. Vander Heyden, "Multiphase Flows and Particle Methods (Part-B)," Annual Conf. of the Computational Fluid Dynamics Society of Canada, British Columbia, Canada (1997).
Kashiwa, B. A., N. T. Padial, R. M. Rauenzahn, and W. B. Vander-Heyden, ASME Symp. on Numerical Methods for Multiphase Flows, Lake Tahoe, Nevada (1994).
Khadilkar, R. M., Y. Wu, M. H. Al-Dahhan, M. P. Dudukovic, and M. Colakyan, "Comparison of Trickle-Bed and Upflow Reactor Performance at High Pressure: Model Predictions and Experimental Observations," *Chem. Eng. Sci.*, **51**, 2139 (1996).
Khadilkar, R. M., M. H. Al-Dahhan, and M. P. Dudukovic, "Parametric Study of Unsteady State Flow Modulation in Trickle Bed Reactors," *Chem. Eng. Sci.*, **54**, 2585 (1999).
Kramer, G. J., "Static Liquid Holdup and Capillary Rise in Packed Beds," *Chem. Eng. Sci.*, **53**, 2985 (1998).
Kuipers, J. A. M., and W. P. M. van Swaaij, "Computational Fluid Dynamics Applied to Chemical Reaction Engineering," *Advances in Chemical Engineering*, Vol. 24, J. Wei et al., eds., Academic Press, New York, p. 227 (1998).
Lage, J. L., "The Fundamental Theory of Flow Through Permeable Media from Darcy to Turbulence," *Transport Phenomena in Porous Media*, D. B. Ingham and I. Pop, eds., Pergamon, New York (1998).
Larachi, F., A. Laurent, N. Midoux, and G. Wild, "Experimental Study of a Trickle-Bed Reactor Operating at High Pressure: Two-Phase Pressure Drop and Liquid Saturation," *Chem. Eng. Sci.*, **46**, 1233 (1991).
Larachi, F., I. Iliuta, M. H. Al-Dahhan, and M. P. Dudukovic, "Discriminating Trickle-Flow Hydrodynamic Models: Some Recommendations," *Ind. Eng. Chem. Res.*, **39**, 4437 (2000).
Latifi, M. A., N. Midoux, and A. Storck, "The Use of Micro-Electrodes in the Study of the Flow Regimes in Packed Bed Reactor with Single Phase Liquid Flow," *Chem. Eng. Sci.*, **44**, 2501 (1989).
Levec, J., K. Grosser, and R. G. Carbonell, "The Hysteretic Behavior of Pressure Drop and Liquid Holdup in Trickle Beds," *AIChE J.*, **34**, 1027 (1988).
Levenspiel, O., *Chemical Reaction Engineering*, 2nd ed., Wiley, New York (1972).
Leverett, M. C., "Capillary Behavior in Porous Solid," *Trans. AIME*, **142**, 159 (1941).
Logtenberg, S. A., and A. G. Dixon, "Computational Fluid Dynamics Studies of Fixed-Bed Heat Transfer," *Chem. Eng. Process*, **37**, 7 (1998).
Lutran, P. G., K. M. Ng, and E. P. Delikat, "Liquid Distribution in Trickle Beds. An Experimental Study Using Computer-Assisted Tomography," *Ind. Eng. Chem. Res.*, **30**, 1270 (1991).
McDonald, L. F., M. S. El-Sayed, K. Mow, and F. A. L. Dullien, "Flow Through Porous Media—The Ergun Equation Revisited," *Ind. Eng. Chem. Fundam.*, **18**, 199 (1979).
Melli, T. R., J. M. Santos, W. B. Kolb, and L. E. Scriven, "Cocurrent Downflow in Networks of Passages: Microscale Roots of Macroscale Flow Regimes," *Ind. Eng. Chem. Res.*, **29**, 2367 (1990).
Mueller, G. E., "Prediction of Radial Porosity Distribution in Randomly Packed Fixed Beds of Uniformly Sized Spheres in Cylindrical Containers," *Chem. Eng. Sci.*, **46**, 706 (1991).
Pan, Y., M. P. Dudukovic, and M. Cheng, "Numerical Investigation of Gas-Driven Flow in 2-D Bubble Columns," *AIChE J.*, **46**, 434 (2000).
Ranade, V. V., "Computational Fluid Dynamics for Reactor Engineering," *Trans. Inst. Chem. Eng.*, **75A**, 14 (1995).
Ravindra, P. V., D. P. Rao, and M. S. Rao, "Liquid Flow Texture in Trickle-Bed Reactors: An Experimental Study," *Ind. Eng. Chem. Res.*, **36**, 5133 (1997).
Reinecke, N., G. Petritsch, D. Schmitz, and D. Mewes, "Tomographic Measurement Techniques—Visualization of Multiphase Flows," *Chem. Eng. Techik.*, **21**, 7 (1998).
Saez, A. E., and R. G. Carbonell, "Hydrodynamic Parameters for Gas-Liquid Cocurrent Flow in Packed Beds," *AIChE J.*, **31**, 52 (1985).
Sederman, A. J., M. L. Johns, A. S. Bramley, P. Alexander, and L. F. Gladden, "Magnetic Resonance Imaging of Liquid Flow and Pore Structure within Packed Beds," *Chem. Eng. Sci.*, **52**, 2239 (1997).
Sederman, A. J., "PDF of Voxel Porosity Distribution," Univ. of Cambridge, Cambridge, England, unpublished (2000).
Sokolichin, A., and G. Eigenberger, "Gas-Liquid Flow in Bubble Columns and Loop Reactors: Part I: Detailed Modeling and Numerical Simulation," *Chem. Eng. Sci.*, **49**, 5735 (1994).

Stanek, V., and J. Szekely, "Three-Dimensional Flow of Fluids Through Nonuniform Packed Beds," *AIChE J.*, **20**, 974 (1974).
Stanek, V., *Fixed Bed Operations: Flow Distribution and Efficiency*, Ellis Horwood Series in Chemical Engineering, Ellis Horwood, New York (1994).
Stephenson, J. L., and W. E. Stewart, "Optical Measurements of Porosity and Fluid Motion in Packed Beds," *Chem. Eng. Sci.*, **41**, 2161 (1986).
Szady, M. J., and S. Sundaresan, "Effect of Boundaries on Trickle-Bed Hydrodynamics," *AIChE J.*, **37**, 1237 (1991).
Tannehill, J. C., D. A. Anderson, and R. H. Pletcher, *Computational Fluid Mechanics and Heat Transfer*, 2nd ed., Taylor & Francis, London (1997).
Trambouze, P., "Computational Fluid Dynamics Applied to Chemical Reaction Engineering," *Rev. Inst. Fr. Pet.*, **48**, 595 (1993).
Tsochatzidis, N. A., and A. J. Karabelas, "Pulsing Flow in Packed Beds: A Method of Process Intensification," *Proc. Int. Conf. on Process Intensification for the Chemical Industry*, BHR Group Conf. Ser. Publ. (McKinseez & Co., Berlin, Germany), **21**(1), 7 (1998).
Wang, Y.-F., Z.-S. Mao, and J.-Y. Chen, "Scale and Variance of Radial Liquid Maldistribution in Trickle Beds," *Chem. Eng. Sci.*, **53**, 1153 (1998).
Wijngaarden, R. J., and K. R. Westerterp, "The Statistical Character of Packed-Bed Heat Transport Problems," *Chem. Eng. Sci.*, **47**, 3125 (1992).
Wu, Y., M. R. Khadilkar, M. H. Al-Dahhan, and M. P. Dudukovic, "Comparison of Upflow and Downflow Two Phase Flow Reactors with and without Fines," *Ind. Eng. Chem. Res.*, **35**, 397 (1996).
Yin, F. H., C. G. Sun, A. Afacan, K. Nandakumar, and K. T. Chung, "CFD Modeling of Mass-Transfer Processes in Randomly Packed Distillation Columns," *Ind. Eng. Chem. Res.*, **39**, 1369 (2000).

Manuscript received Mar. 23, 2001, and revision received Sept. 10, 2001.